ISSN 1064-2269, Journal of Communications Technology and Electronics, 2022, Vol. 67, No. 9, pp. 1105–1112. © Pleiades Publishing, Inc., 2022.
Russian Text © The Author(s), 2022, published in Radiotekhnika i Elektronika, 2022, Vol. 67, No. 9, pp. 900–907.

THEORY AND METHODS OF SIGNAL PROCESSING

Formation of Two-Color Radiation with Controlled Rotation of the Polarization Plane

V. M. Kotov*

Kotelnikov Institute of Radioengineering and Electronics (Fryazino Branch), Russian Academy of Sciences, Fryazino, Moscow oblast, 141190 Russia

**e-mail: vmk277@ire216.msk.su*

Received November 9, 2021; revised April 25, 2022; accepted April 27, 2022

Abstract—A method is proposed for the formation of two-color optical radiation with a rotating polarization vector, the rotation frequency of which is determined by the acoustic frequency. The method is based on acousto-optic (AO) diffraction of two-color radiation by an acoustic wave and the interference of circularly polarized beams with different frequencies. The rotation of polarization of two-color radiation is experimentally demonstrated for wavelengths of 0.488×10^{-4} and 0.514×10^{-4} cm using two AO Bragg cells made of a gyrotropic TeO_2 crystal. Polarization rotation with a frequency of about 109 MHz is obtained.

DOI: 10.1134/S106422692209008X

INTRODUCTION

Acousto-optic (AO) diffraction is widely used to control the parameters of an optical wave. The most popular in practice is the Bragg diffraction, which allows deflection of up to 100% of radiation to a single diffraction order [1, 2]. However, this mode is highly selective with respect to the optical wavelength, which, until recently, made it difficult to use it to control, for example, two-color radiation. Nevertheless, several diffraction regimes provide the Bragg matching of two arbitrary optical waves with one acoustic wave. Normally, such regimes are implemented at certain acoustic frequencies that depend on the optical wavelengths and polarizations [3]. Two-color radiation is currently widely employed in practice: it allows the analysis of the dispersion properties of liquid crystals [4], complex molecular compounds [5], and optically active medicines, sugars [6], etc. Application of the methods to control two-color radiation makes it possible to construct two-color polarimeters for the simultaneous measurements of the polarization characteristics of transparent media at two wavelengths. Two-color radiation is employed in Doppler anemometry [7–10], in the design of fiber-optic gyroscopes [11, 12], etc.

Note that the existing methods make it possible to form a rotating polarization vector of monochromatic radiation (see, for example, [13]), with the rotation frequency depending on the frequency of the acoustic wave. Polarization rotation frequencies equal to two and four acoustic frequencies have experimentally obtained in [14–16]. Radiation with a rotating polarization vector is used, for example, for high-frequency amplitude modulation of the beam with the modulation frequency that is several times greater than the pulse modulation frequency [17]. However, only monochromatic radiation has been considered in all previous works.

The purpose of this work is to create a method for the formation of two-color radiation with a rotating polarization vector. This will substantially facilitate the application of two-color radiation in various problems and provide formation of controlled rotation of the polarization vector of two-color radiation.

1. THEORY

Figure 1 shows the vector diagram of the proposed method based on a variant of the AO-diffraction of two-color radiation. The diffracted beams must propagate on one side of the incident radiation (see below). In Fig. 1, the original two-color radiation is represented using collinearly directed wave vectors $\vec{K}$ and $\vec{T}$, which describe the propagation of beams with wavelengths λ_1 and λ_2, respectively, in air. The radiation is incident at angle γ on input face OX of a uniaxial crystal. The OX face is oriented orthogonally to the crystal optical axis oz. Inside the crystal, each monochromatic component is refracted and split into two eigenwaves: wave $\vec{K}$ into $\vec{K}_1$ and $\vec{K}_2$, propagating at angles φ_1 and φ_2 relative to the oz axis, respectively, and wave $\vec{T}$ into $\vec{T}_1$ and $\vec{T}_2$, the angles between which and the oz axis are θ_1 and θ_2. Here, waves $\vec{K}_1$ and $\vec{T}_1$ belong to the internal surfaces of the wave vectors of the crystal, and waves $\vec{K}_2$ and $\vec{T}_2$ belong to the external surfaces. An acoustic wave with wave vector $\vec{q}$ propa-

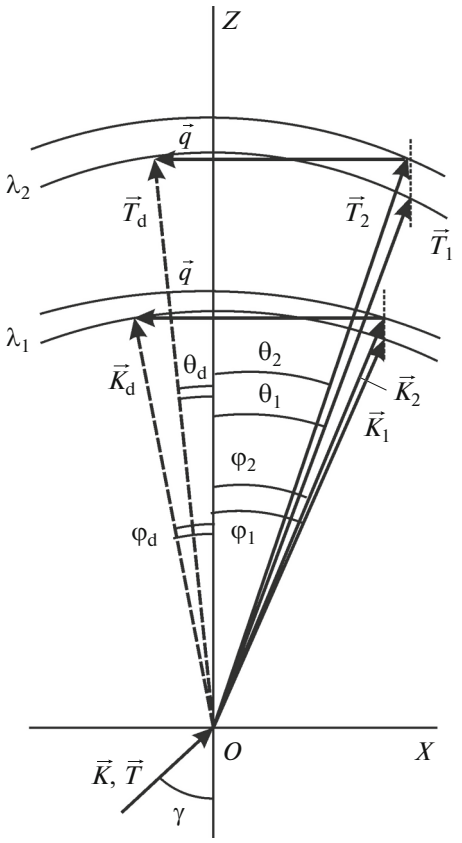

Fig. 1. Vector diagram of the AO diffraction of the two-color radiation by a single acoustic wave (the dashed lines show the diffracted beams).

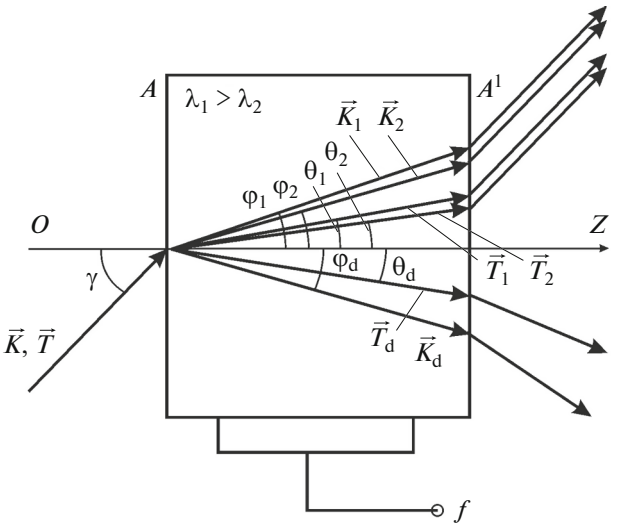

Fig. 2. Beam paths in the AO cell.

gates orthogonally to the *oz* axis. Anisotropic diffraction takes place: beam $\vec{K}_2$ is diffracted along the direction of beam $\vec{K}_d$ and beam $\vec{T}_2$ is diffracted along the direction of beam $\vec{T}_d$. The angles between $\vec{K}_d$, $\vec{T}_d$ and the *oz* axis are φ_d and θ_d. Beams $\vec{K}_1$ and $\vec{T}_1$ propagate through the crystal without diffraction and merge into one beam at the exit from the crystal. In general, diffracted beams $\vec{K}_d$ and $\vec{T}_d$ do not merge with each other at the exit from the crystal and propagate at different angles.

Figure 2 shows the beam paths in the AO cell (the notation corresponds to that of Fig. 1). Here, two-color radiation $\vec{K}, \vec{T}$, with wavelengths λ_1 and λ_2 ($\lambda_1 > \lambda_2$) is incident on optical face *A* of the cell. An acoustic wave excited at frequency *f* propagates in the crystal. Inside the crystal, the incident radiation is split into two pairs of monochromatic beams: $\vec{K}_1$ and $\vec{K}_2$ ("ordinary" and "extraordinary" with wavelength λ_1) and $\vec{T}_1$ and $\vec{T}_2$ ("ordinary" and "extraordinary" with wavelength λ_2). Diffracted beams are $\vec{T}_d$ and $\vec{K}_d$. Optical faces of the crystal *A* and A^1 are parallel to each other and orthogonal to optical axis *oz*.

A uniaxial gyrotropic TeO_2 crystal, which is most widely used in practice, serves as the AO medium. The refractive indices of such a crystal are given by [3, 18]

$$n_{1,2}^2 = \frac{1+\tan^2\varphi}{\frac{1}{n_0^2}+\frac{\tan^2\varphi}{2}\left(\frac{1}{n_0^2}+\frac{1}{n_e^2}\right)\pm\frac{1}{2}\sqrt{\tan^4\varphi\left(\frac{1}{n_0^2}-\frac{1}{n_e^2}\right)^2+4G_{33}^2}}, \quad (1)$$

where n_0, n_e are the principal refractive indices of the crystal, φ is the angle between optical axis *OZ* of the crystal and wave vector of the optical wave, and G_{33} is the component of the gyration pseudotensor.

Specific values are determined for the two-color radiation of an Ar-laser. The radiation is diffracted by an acoustic wave that propagates in the TeO_2 crystal. The speed of sound in the crustal is $V = 0.617 \times 10^5$ cm/s.

Using the results of [19, 20] for TeO_2, we obtain:

$$\lambda_1 = 0.5145\times10^{-4}\ \text{cm};\quad n_0 = 2.3115;\quad n_e = 2.4735;\quad g_{33} = 3.69\times10^{-5};$$

$$\lambda_2 = 0.488\times10^{-4}\ \text{cm};\quad N_0 = 2.3303;\quad N_e = 2.494;\quad G_{33} = 3.93\times10^{-5}.$$

Calculations show that the AO diffraction of two-color Ar-laser radiation in the TeO_2 crystal (Fig. 1) occurs in a frequency interval of 102–116 MHz at a level of 3 dB with a central frequency of $f = 109$ MHz.

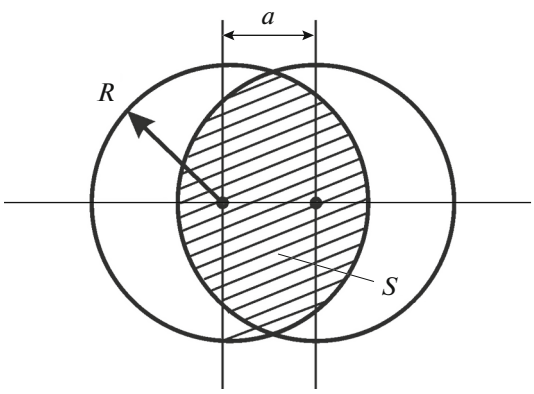

Fig. 3. Overlapping of intersecting beams: R, radius of circle; S, area of the region of intersection; and a, distance between the centers of circles.

An angle of incidence of light on the crystal of $\gamma = 3.25°$ corresponds to the central frequency. Inside the crystal, the beam with wavelength λ_1 is split into two beams, which are refracted at angles φ_1 and φ_2, such that $\varphi_1 \approx \varphi_2 \approx \gamma/n_0 = 1.41°$ and the difference between the angles is $\Delta\varphi = \varphi_1 - \varphi_2 = 3.1 \times 10^{-4}$ deg. The radiation with wavelength λ_2 is also split into two beams, which are refracted at angles $\theta_1 \approx \theta_2 \approx \gamma/N_0 = 1.39°$ and the difference is $\Delta\theta = \theta_1 - \theta_2 = 2.9 \times 10^{-4}$ deg. Such small splitting angles $\Delta\varphi$ and $\Delta\theta$ of monochromatic pairs are due to the fact that the beams propagate near the optical axis, where the anisotropy of the crystal almost vanishes, so that the splitting of the monochromatic components is absent. The difference of the angles of propagation of the beams with different wavelengths is noticeable (0.02°), but is almost unobservable due to the superposition of the apertures of the beams.

We consider the superposition of the apertures and estimate the degree of overlapping of two beams depending on the distance between the centers of the beams. Figure 3 shows the cross section of two intersecting beams. We assume that the cross sections of both beams are circles with identical radii R. The circles are superimposed, and the distance between the centers of the circles is a. The intersection area of the circles is S. Area S is calculated as

$$S = 2R\left(R\varphi - 0.5aR\sin\varphi\right), \quad (2)$$

where $\varphi = \arccos(0.5a/R)$. Degree of overlapping of the two circles μ is defined as the ratio of area S to the circle area:

$$\mu = S/\pi R^2. \quad (3)$$

It is clear that an increase in the propagation distance of the beams leads to an increase in distance a between the centers, a decrease in S, and, hence, a decrease in μ. The distance between the centers can be estimated as $a \sim L\Delta\eta$, where L is the optical path and $\Delta\eta$ is the angle of divergence of the beams (in radians). We assume that that the dimension of the crystal along the beam propagation is 10 mm (the dimension of the crystal in the experiments). Then, parameter a_k for diverging beams $\vec{K}_1,\vec{K}_2$ is $a_k = L\Delta\varphi = 5.4 \times 10^{-6}$ mm, and parameter a_T for divergent beams $\vec{T}_1,\vec{T}_2$ is $a_T = L\Delta\theta = 5.0 \times 10^{-6}$ mm. In other words, the monochromatic beams are not split. The divergence of the beams with different wavelengths λ_1 and λ_2 having passed the same distance (10 mm) is estimated as $a_{kT} = L(\varphi_1 - \theta_1) = 3.5 \times 10^{-3}$ mm. Using expressions (2) and (3), we obtain $\mu = 0.9967$. Thus, the beams of different colors are almost completely overlapped.

The beam separation was verified in experiments. Figures 4a and 4b show photographs of laser beam spots for the AO diffraction observed on a screen located at distances of 80 and 10 cm from the AO cell, respectively. The camera was also located at different distances from the screen (80 and 30 cm, respectively), so that the sizes of the photographs are different. The radiation source is an Ar-laser with the highest radiation intensities at wavelengths 0.514 μm (green line, G) and 0.488 μm (blue line, B). A slow transverse acoustic wave with a frequency of 109 MHz and a propagation

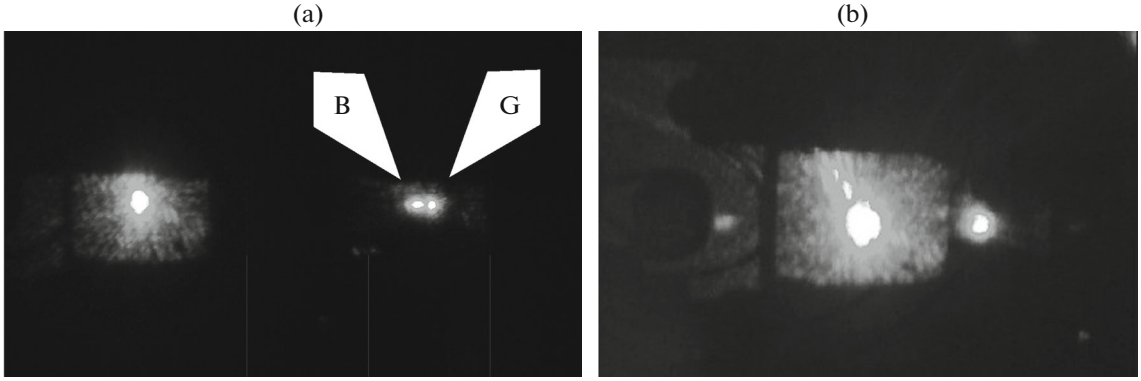

Fig. 4. Photographs of the G and B spots on the screen located at distances of (a) 80 and (b) 10 cm from the AO cell.

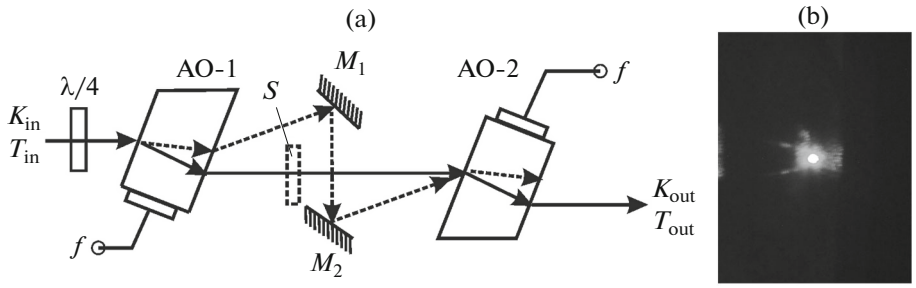

Fig. 5. (a) Optical scheme of the experimental setup and (b) photographs of the diffraction spots at a distance of 80 cm from the screen to the second AO cell: K_{in}, T_{in}, two-color input radiation; K_{out}, T_{out}, two-color output radiation; M_1 and M_2 , mirrors; S, shutter; (dashed arrows) diffracted radiation; and (solid lines) nondiffracted radiation.

speed of 617 m/s was excited in the AO (paratellurite) crystal. The left-hand side of Fig. 4a shows the nondiffracted beams (in fact, the superposition of two beams with wavelengths λ_1 and λ_2) and the right-hand side shows the diffracted beams split into monochromatic components. It is clearly seen that the nondiffracted radiation is represented as a single spot, while the diffracted radiation is represented as two spots B and G. Spot G is deflected stronger than spot B in accordance with the theory of the AO diffraction. Direct measurements show that the angle between the diffracted beams is about 0.2°. The central part of Fig. 4b shows the nondiffracted radiation, and the diffracted beams are shown on the right- and left-hand sides. The background around the central spot is due to the scattering of light in the crystal of the AO cell. The cell is close to the screen, so that the parasitic scattering is observed on the screen. The main diffraction order is the right-hand spot, which is much brighter than the left-hand one. It is seen that beams B and G are not split in this order.

Figure 5a shows the optical scheme of the device that is used to form the rotating polarization vector. Here, the fundamental point is that two AO cells are made of a TeO_2 crystal, which is gyrotropic, so that its eigenwaves propagating along the optical axis are circularly polarized. Upon deflection from the optical axis, the polarizations become elliptical. The ellipticity of the eigenwaves of the crystal is calculated as

$$\rho = \frac{1}{2G_{33}} \times \left[\sqrt{\tan^4\varphi\left(\frac{1}{n_0^2}-\frac{1}{n_e^2}\right)^2 + 4G_{33}^2} - \tan^2\varphi\left(\frac{1}{n_0^2}-\frac{1}{n_e^2}\right)\right]. \quad (4)$$

The ellipticities of the beams with wavelengths λ_1 and λ_2 are $\rho_1 = 0.82$ and $\rho_2 = 0.84$, respectively. It is seen that the ellipticities of the beams are quite high (close to unity). The closeness of ellipticities to unity is fundamentally important for the formation of radiation with a rotating polarization vector (see below).

In Fig. 5a, the input two-color radiation is K_{in}, T_{in} and the output radiation is K_{out}, T_{out}. The input radiation passes through an achromatic quarter-wave retardation plate $\lambda/4$ and two cells AO-1 and AO-2, made of a gyrotropic crystal, in which acoustic waves have identical frequencies but opposite directions of propagation. Mirrors M_1 and M_2 provide parallel shift of the diffracted beams into the region of intersection with the nondiffracted radiation.

The distance that the diffracted beams pass from the AO-1 cell to the AO-2 cell, being reflected on their way from mirrors M_1 and M_2, is about 10 cm. The angle between the diffracted beams is 0.2°, so that the distance between the beam centers is $a = 0.35$ mm for beam paths of 10 cm. For such a distance, the degree of overlapping is $\mu = 0.67$. After diffraction in the AO-2 cell, the diffracted beams propagate parallel to each other. The degree of overlapping of the diffracted beams remains unchanged (0.67).

Figure 5b shows a photograph of the diffracted beams observed on the screen with the nondiffracted beams blocked by shutter S (see Fig. 5a). The distance from the second AO cell to the screen is 80 cm. It is seen that the beams almost merge into one beam after the second diffraction. In the absence of shutter S, the brightness of the spot will simply increase due to the contribution of the nondiffracted radiation.

The system with two mirrors makes it possible to restore the polarization of the radiation incident on the mirrors, which is a necessary condition for the interference leading to the formation of a rotating polarization vector. Indeed, after the first reflection, for example, the left-hand circular polarization becomes right-hand and, after the second reflection, the polarization again becomes left-hand circular. The right-hand circular polarization is transformed similarly. In the first cell, diffraction occurs from the zero order to the first one, and in the second cell, vice versa, from the first order to the zero one, so that, at a diffraction efficiency of 100% in each cell, all radiation returns to the original beam. If the frequencies of the diffracted beams increase by Ω (Ω is the acoustic frequency) in the first cell, the frequencies of the re-dif-

fracted beams will increase by 2Ω in the second cell. Thus, the output radiation is formed from nondiffracted beams with frequencies ω_1 and ω_2 (ω_1 and ω_2 are the frequencies of beams with wavelengths λ_1 and λ_2, respectively) and diffracted beams with frequencies $(\omega_1 + 2\Omega)$ and $(\omega_2 + 2\Omega)$. The waves involved in the process have circular polarizations: for example, nondiffracted waves (with frequencies ω_1 and ω_2) are right-hand circular waves and diffracted waves (with frequencies $(\omega_1 + 2\Omega)$ and $(\omega_2 + 2\Omega)$) are left-hand circular waves. Thus, the summation of these waves will lead to the formation of linearly polarized waves and the polarization plane of each component will rotate at frequency Ω [21]. Hence, a linearly polarized two-color radiation is formed and its polarization plane rotates at a frequency determined by the acoustic frequency.

It follows from the working principle of the device that the effect is due to the summation of two beams with different frequencies. It is known that the greatest depth of interference is reached when the amplitudes of the interfering beams are equal. However, we consider the beams that are twice diffracted by the acoustic waves and the beams that pass through the device without diffraction. In practice, it is impossible to achieve a diffraction efficiency of 100% owing to the radiation scattering into higher diffraction orders, inhomogeneity of optical and acoustic waves, etc. In addition, we can hardly provide complete identity of two cells, so that the maximum diffraction efficiencies are obtained at different levels of acoustic power.

To equalize the intensities of the diffracted and nondiffracted beams, we propose application of a quarter-wave retardation plate at the entrance to the device. Variations in the orientation of the plate, lead to variations in the ratio of the amplitudes of the eigenwaves of the gyrotropic crystal. To prove this, we choose coordinate system (x, y, z) related to the $\lambda/4$ plate, with the z axis coinciding with the normal to the optical faces of the plate and the x and y axes directed along the fast and slow axes. We assume that linearly polarized monochromatic radiation is incident on the plate and the polarization plane makes angle α, for example, with the fast axis of the plate (i.e., the x axis). Then, having passed through the plate, the radiation becomes elliptically polarized with field amplitudes along the x and y axes given by

$$E_x = A\cos(\omega t), \quad E_y = B\sin(\omega t), \tag{5}$$

where $A = E_0\cos\alpha$ and $B = E_0 \sin\alpha$. Here, E_0 is the field amplitude of the linearly polarized beam incident on the plate, ω is the optical frequency, and t is the time. In the gyrotropic crystal, radiation (5) is split into two circularly polarized eigenwaves with amplitudes a (right-hand) and b (left-hand) [22]:

$$E_{x1} = a\cos(\omega t), \quad E_{y1} = a\sin(\omega t), \tag{6}$$

$$E_{x2} = b\cos(\omega t), \quad E_{y2} = -b\sin(\omega t). \tag{7}$$

Owing to the conservation of the fields along the x and y axes, we have

$$E_x = E_{x1} + E_{x2}; \quad E_y = E_{y1} + E_{y2}, \tag{8}$$

and amplitudes a and b of the eigenwaves in the crystal are calculated as

$$a = \frac{E_0}{\sqrt{2}}\cos\left(\alpha - \frac{\pi}{4}\right), \quad b = \frac{E_0}{\sqrt{2}}\sin\left(\alpha - \frac{\pi}{4}\right). \tag{9}$$

Expression (9) shows that a variation in angle α (i.e., variation in the orientation of the $\lambda/4$ plate) makes it possible to equalize the amplitudes of the diffracted and nondiffracted beams and, hence, improve the characteristics of the output radiation with a rotating polarization vector. It is clear that an achromatic $\lambda/4$ plate must be used for the two-color radiation. Such plates are commercially available (see, for example, https:// phcloud.ru/index.php/catalog/optika/chetvert-volnovye-plastiny) and can be easily purchased and employed.

A device for the formation of the two-color radiation with a rotating polarization vector is supposed to be used in systems for two-coordinate anemometry. It is of interest to compare the characteristics of anemometers using the rotating polarization and the differential optical scheme that is widely employed in practice. We consider single-coordinate schemes of the two variants. Figure 6a shows a differential scheme for the formation of a probing volume [7–9] that results from the interference of two beams *1* and *2* intersecting at angle η. An interference pattern with the period $d = \lambda/2\sin\eta$ is formed in the intersection region. A particle crossing the interference field scatters light in each layer of the pattern. Photodetector *PD* records scattered light as a series of electric pulses. Figure 6b shows the scheme in which a particle crosses a beam with a rotating polarization vector, the aperture of which is also D. The polarization rotation frequency is determined by acoustic frequency f. In both cases, photodetector *PD* detects the field scattered by the particle in the form of a series of electric signals (Figs. 6c and 6d). In both cases, the projection of velocity V along the x axis, orthogonal to the probing volumes, is defined as

$$V_x = D/n\Delta t,$$

where Δt is the time interval between the neighboring pulses and n is the number of pulses. However, a variation in the speed of particle leads to a variation in time interval Δt in the differential scheme, while the number of pulses remains unchanged. In the scheme with the rotating polarization vector, time interval Δt remains unchanged and number of pulses n is changed.

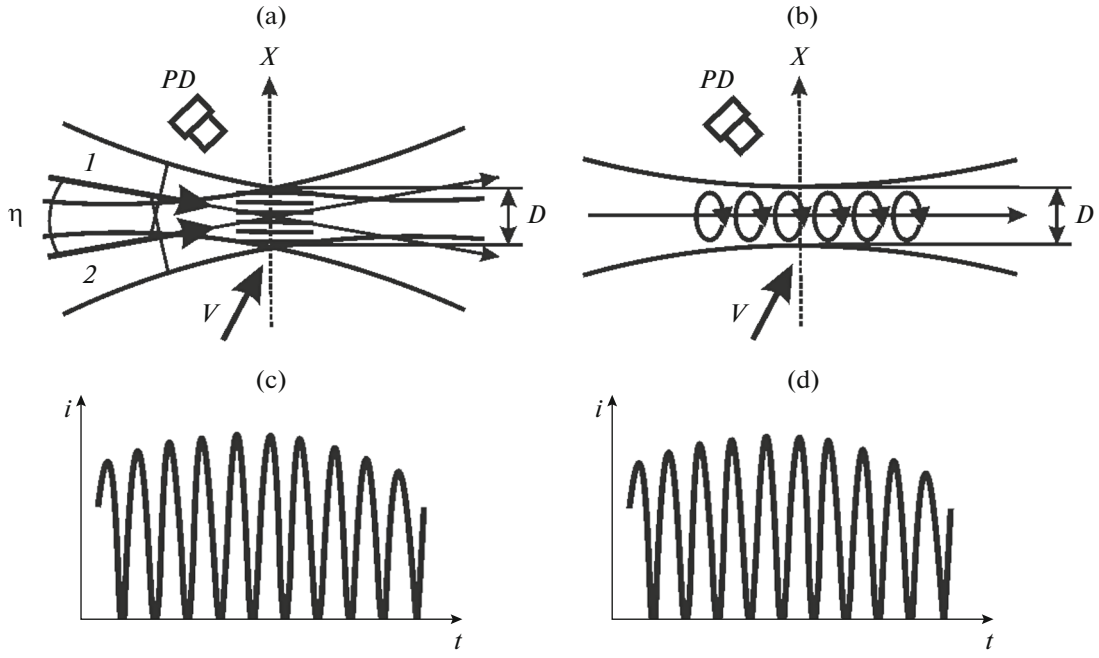

Fig. 6. Comparison of (a) differential scheme and (b) scheme with the rotating polarization vector for the measurement of the speed of particle and (c) and (d) measured signals for schemes (a) and (b), respectively: (*1*) and (*2*) beams, *D* beam aperture, and *PD* photodetector.

2. EXPERIMENTAL RESULTS AND DISCUSSION

An experiment was performed to verify the results. Figure 5a presents the experimental scheme. An Ar-laser generating linearly polarized radiation with the highest intensities at wavelengths of $\lambda_1 = 0.514 \times 10^{-4}$ cm and $\lambda_2 = 0.488 \times 10^{-4}$ cm (green (G) and blue (B) lines) serves as the source of radiation. Two identical paratellurite AO cells with dimensions of 0.8, 0.8, and 1.0 cm along the [110], [1 $\bar{1}$0], and [001] crystal directions, respectively, are used in the experiment. The [001] direction is the *oz* optical axis of the crystal. A transverse acoustic wave with a velocity of 617 m/s is generated along the [110] direction coinciding with the *ox* axis (Fig. 1). The cells are oriented in such a way that the acoustic waves in them propagate in opposite directions. Both cells were supplied with electric signals from a single generator. The signal voltage of the generator is about 8 V at a load of 50 Ω. The acoustic frequency is 109 MHz. The bandwidth of the piezoelectric transducer is about 2 MHz. Such a narrow band is due to the fact that the fifth harmonic of the transducer is used. In the experiments, we use the Bragg diffraction regime, in which both beams are simultaneously diffracted by the same acoustic wave. The laser radiation passes, first, through a polarizer serving as a radiation attenuator and, then, through an achromatic quarter-wave retardation plate to obtain the maximum modulation depth. After that, the radiation passes through another polarizer, which serves as an analyzer of the rotation of the polarization plane. The output radiation is directed to a photodetector the electric signal from which is sent to an oscilloscope. Components with wavelengths λ_1 and λ_2 are measured independently with the aid of interference filters. Figure 7 presents the signals corresponding to modulation of the G (curve *1*) and B (curve *2*) radiation. We also present the zero signal (curve *3*) recorded in the

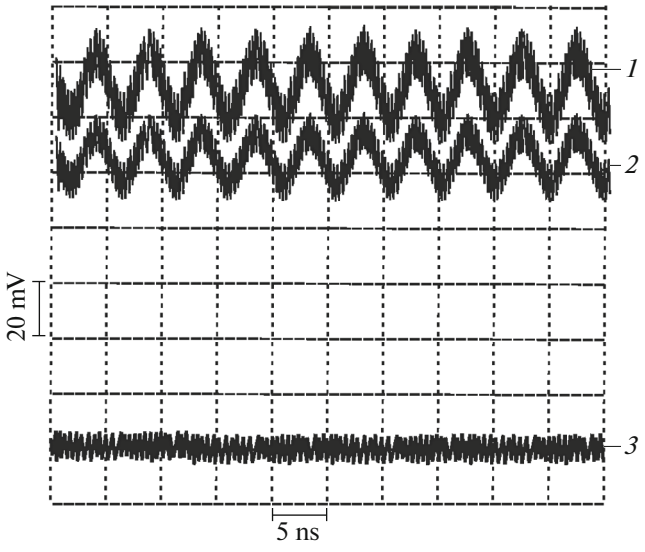

Fig. 7. Oscilloscope signals: (*1*) and (*2*) modulation signals of the G and B beams and (*3*) zero signal of the photodetector.

absence of optical radiation. All signals exhibit a noise component corresponding to the noise of the photodetector. The frequencies of signals *1* and *2* correspond to two frequencies of the signal applied to the AO cell, which is proven by frequency measurements using a frequency meter. Different levels of the signals are due to the fact that the intensity of the green line of the laser is greater (by about 20%) than the intensity of the blue line. The true frequency of the polarization rotation is 109 MHz, since the photodetector works in the quadratic mode and doubles the signal frequency. The signal modulation depth is 15–20% depending on the analyzer orientation. In other words, the output signal exhibits ellipticity.

A relatively small depth of the signals in Figs. 7 can be due to several factors: incomplete overlapping of interfering beams, incomplete identity of the AO cells (electric and acoustic characteristics), inhomogeneity of the cell material, and inaccurate orientation of the faces relative to the crystallographic axes. In addition, the optical paths of the transmitted and diffracted beams twice reflected from the mirrors are different, so that the phase noise of the laser can be manifested [24]. The result of interference is also affected by the fact that the polarizations of the waves are, strictly speaking, elliptical rather than circular, which worsens the interference contrast. Note that, in devices that employ monochromatic radiation, the depth of interference in differential schemes amounts to 30% [25]. In our experiments, such a depth can also be reached but only for one monochromatic component with the worsening for the other. This is quite simply achieved using the alignment of mirrors M_1 and M_2. Figure 7 presents the optimal mode, in which the modulation depths of both components are identical (about 20%). The proposed scheme is quite simple but, at the same time, new and interesting, since it allows formation of two-color radiation with a rotating polarization vector.

CONCLUSIONS

Thus, the results make it possible to draw the following conclusions.

The two-color optical radiation with a rotating polarization vector can be formed using the AO diffraction, in which both monochromatic components are diffracted on the same side of the incident radiation. A gyrotropic crystal the eigenwaves of which are circularly polarized can be used as the AO medium.

A scheme of AO diffraction based on two identical AO cells working at the same acoustic frequency has been proposed. Two mirrors are used to direct the radiation diffracted in the first cell to the second cell at the same angle to the region of intersection with the nondiffracted part of the radiation. Two mirrors make it possible to restore the polarization of the radiation incident on the mirrors, thereby providing the best conditions for the formation of the rotating polarization vector.

We have calculated the parameters of the scheme using a paratellurite crystal as the AO medium. It has been shown that the two-color radiation with wavelengths of 0.514×10^{-4} and 0.488×10^{-4} cm is efficiently diffracted by the slow acoustic wave with a frequency of 109 MHz at a bandwidth of 15 MHz at a level of 3 dB.

The scheme has been tested using a device consisting of two consecutive paratellurite AO cells working at an acoustic frequency of 109 MHz. The radiation of an Ar-laser at wavelengths of 0.514×10^{-4} and 0.488×10^{-4} cm has been used as the two-color radiation. Polarization rotation of the two-color radiation at a frequency of about 109 MHz has been obtained.

FUNDING

This work was supported by the State Contract of the Kotelnikov Institute of Radioengineering and Electronics.

CONFLICT OF INTERESTS

The author declares that he has no conflicts of interest.

REFERENCES

1. V. I. Balakshii, V. N. Parygin, and L. E. Chirkov, *Physical Principles of Acousto-Optics* (Radio i Svyaz', Moscow, 1985) [in Russian].
2. J. Xu and R. Stroud, *Acousto-Optic Devices: Principles, Design and Applications* (Wiley, New York, 1992).
3. V. M. Kotov, *Acousto-Optics. Bragg Diffraction of Multi-Color Radiation* (Yanus-K, Moscow, 2016) [in Russian].
4. E. A. Konshina and D. S. Kostomarov, Opt. Zh., No. 10, 88 (2007).
5. G. F. Kolbina, A. E. Grishchenko, Yu. N. Sazanov, and I. N. Shtennikova, Vysokomol. Soedin. Ser. A **51**, 1104 (2009).
6. *Pharmaceutical Chemistry: Textbook*, Ed. by G. V. Ramenskaya (Binom. Lab. Znanii, Moscow, 2015) [in Russian].
7. V. S. Rinkevichus, *Laser Anemometry* (Energiya, Moscow, 1978).
8. V. P. Koronkevich and V. A. Khanov, *Modern Laser Interferometers* (Nauka, Novosibirsk, 1985).
9. V. P. Klochkov, L. F. Kozlov, I. V. Potykevich, and M. S. Soskin, *Laser Anemometry, Remote Spectroscopy, and Interferometry. Reference Book* (Naukova Dumka, Kiev, 1985).
10. S. N. Antonov, V. M. Kotov, and V. N. Sotnikov, Zh. Tekh. Fiz. **61**, 161 (1991).
11. A. D. Kersey, A. Dandridge, and W. K. Burns, Electron. Lett. **22**, 935 (1986).
12. V. M. Kotov, Kvant. Elektron. **24**, 471 (1997).
13. J. Shamir and Y. Fainman, Appl. Opt. **21**, 364 (1982).

14. V. M. Kotov, S. V. Averin, E. V. Kotov, et al. Kvant. Elektron. **47**, 135 (2017).

15. V. M. Kotov and E. V. Kotov, Opt. Zh. **84** (6), 51 (2017).

16. V. M. Kotov and E. V. Kotov, Kvant. Elektron. **48**, 773 (2018).

17. V. M. Kotov, S. V. Averin, and E. V. Kotov, Opt. Zh. **86** (3), 3 (2019).

18. V. M. Kotov, Opt. Spektrosk. **74**, 493 (1994).

19. *Acoustic Crystals*, Ed. by M. P. Shaskol'skaya (Nauka, Moscow, 1982) [in Russian].

20. V. A. Kizel' and V. I. Burkov, *Gyrotropy of Crystals* (Nauka, Moscow, 1980) [in Russian].

21. J. F. Nye, *Physical Properties of Crystals: Their Representation by Tensors and Matrices* (Clarendon Press, Oxford, 1957; Mir, Moscow, 1967).

22. M. Born and E. Wolf, *Principles of Optics: Electromagnetic Theory of Propagation, Interference, and Diffraction of Light* (Pergamon, Oxford, 1964; Nauka, Moscow, 1973).

23. B. Cretin, W.-X. Xie, S. Wang, and D. Hauden, Opt. Commun. **65** (3), 157 (1988).

24. V. A. Grechikhin, *Development and Analysis of Computer Algorithms for Processing of One-Particle Signals of Laser Doppler Anemometers* Cand. Sci. (Tech. Sci.) Dissertation (MEI, Moscow, 1996).

Translated by A. Chikishev